HHS Public Access

Author manuscript

Neuroimage. Author manuscript; available in PMC 2018 February 01.

Published in final edited form as:

Neuroimage. 2017 February 01; 146: 1128–1141. doi:10.1016/j.neuroimage.2016.10.005.

Mapping White-Matter Functional Organization at Rest and during Naturalistic Visual Perception

Lauren Marussich[1], **Kun-Han Lu**[2], **Haiguang Wen**[2], and **Zhongming Liu**[1,2,3,*]

[1]Weldon School of Biomedical Engineering, Purdue University, West Lafayette, IN, USA

[2]School of Electrical and Computer Engineering, Purdue University, West Lafayette, IN, USA

[3]Purdue Institute for Integrative Neuroscience, Purdue University, West Lafayette, IN, USA

Abstract

Despite wide applications of functional magnetic resonance imaging (fMRI) to mapping brain activation and connectivity in cortical gray matter, it has rarely been utilized to study white-matter functions. In this study, we investigated the spatiotemporal characteristics of fMRI data within the white matter acquired from humans in the resting state or watching a naturalistic movie. By using independent component analysis and hierarchical clustering, resting-state fMRI data in the white matter were denoised and decomposed into spatially independent components, further assembled into hierarchically organized axonal fiber bundles. Interestingly, such components were partly reorganized during natural vision. Relative to the resting state, the visual task specifically induced a stronger degree of temporal coherence within the optic radiations, as well as significant correlations between the optic radiations and multiple cortical visual networks. Therefore, fMRI contains rich functional information about activity and connectivity within white matter at rest and during tasks, challenging the conventional practice of taking white-matter signals as noise or artifacts.

Introduction

Since its inception, functional magnetic resonance imaging (fMRI) has been focused on mapping activations and connections in the cerebral gray matter (GM) (Bandettini et al. 1992; Kwong et al. 1992; Ogawa et al. 1992; Biswal et al. 1995; Fox and Raichle 2007). It has had limited use in investigating the functional dynamics and organization of the cerebral white matter (WM) (Gawryluk et al. 2014). This paucity of WM fMRI literature is disproportional considering that WM occupies about half of the human brain volume, contains structural pathways for long-range signaling (Sporns et al. 2005), and has critical implications for numerous neurological diseases (Ffytche and Catani 2005).

It has been often assumed that WM lacks the typical hemodynamic changes driven by neural activity (Logothetis and Wandell 2004). Relative to GM, WM has much lower cerebral vascular density (Lierse and Horstmann 1965), blood volume (Jensen et al. 2006), and blood

*Correspondence. Zhongming Liu, PhD, Assistant Professor of Biomedical Engineering, Assistant Professor of Electrical and Computer Engineering, College of Engineering, Purdue University, 206 S. Martin Jischke Dr., West Lafayette, IN 47907, USA, Phone: +1 765 496 1872, Fax: +1 765 496 1459, zmliu@purdue.edu.

flow (Van Osch et al. 2009). Moreover, energy consumption in WM is about one fourth that of GM overall (Logothetis and Wandell 2004), with more energy used on action potentials rather than synapses (Harris and Attwell 2012). While neurometabolic and neurovascular coupling in WM is also unclear (Logothetis and Wandell 2004), previous findings about the relationship between neural and hemodynamic activities are all based on signals specific to GM (Logothetis et al. 2001; Smith et al. 2002). It is problematic to simply extrapolate such findings either for or against the validity of WM fMRI. Furthermore, artifacts of motion (Johnstone et al. 2006), partial-volume (Jo et al. 2010), and physiological origin (Makedonov et al. 2015) are also of concern in WM fMRI. Hence, the fMRI signal in WM has an unclear basis and an inherently low signal to noise ratio (SNR); as such, it has been dismissed from analysis or interpretation in the vast majority of fMRI studies.

However, increasing evidence has shed light on the feasibility of using fMRI to map WM activation and connectivity. See Gawryluk et al. (2014) for a review. Previous studies showed that inter-hemispheric transfer tasks could induce fMRI activations in the corpus callosum (Tettamanti et al. 2002; Fabri et al. 2011; Gawryluk et al. 2011), through which activated cortical regions were structurally connected across hemispheres (Mazerolle et al. 2010). Such callosal activations may have a metabolic basis, since local cerebral metabolic rate for glucose was found to depend on neural activity in the corpus callosum given graded intra-cortical electrical stimuli (Weber et al. 2002). Beyond the corpus callosum, WM activations have rarely been reported in fMRI studies (Mosier et al. 1999; Mazerolle et al. 2013). Astafiev et al. have demonstrated that symptomatic chronic mTBI subjects show abnormal neural activation during visual tracking tasks in a common set of subcortical and white matter regions using BOLD fMRI acquisitions (Astafiev et al. 2015; Astafiev et al. 2016). Moreover, Ding et al. reported that resting-state fMRI signals in WM were correlated over long distances, as well as locally in a similar anisotropic manner as observed with diffusion tensor imaging (DTI). Although all prior studies that reported WM-fMRI activations were based on T_2*-weighted MRI sequences, the WM-fMRI signal and its correlational structure were recently shown to be blood oxygenation level dependent (BOLD) (Ding et al. 2016). This finding is important since T_2*-weighted signal fluctuation may arise from both BOLD and non-BOLD origins: the former reflects changes in R_2*, the latter may reflect changes in initial signal intensity (S_0) likely due to nuisance effects, e.g. motion and physiological noises (Kundu et al., 2012). Collectively, these studies suggest that there is no fundamental barrier for which fMRI is doomed to fail for functional imaging in WM, paving the way for an emerging domain of fMRI methodologies and applications.

Perhaps the most critical and practical challenge is the much lower dynamic range in WM (i.e. versus that in GM). When univariate or multivariate time-series analyses are applied to GM and WM voxels together, signal variance and structure are dominated by voxels in GM, whereas activity and connectivity patterns in WM are likely under-detected or mistaken as noise. One potential way to deal with this issue is to separate WM from GM and use data-driven analysis, e.g. independent component analysis (ICA), to characterize the spatiotemporal patterns of signal vs. noise exclusively in the WM. This is helpful especially for the resting state, since the absence of any overt task makes it more difficult to discriminate signal from noise without any presumed temporal characteristics. A plausible criterion to distinguish signal from noise is based on their expected difference in

reproducibility within and across subjects. The brain's structural and functional organization is generalizable and stable, serving as the underlying constraint for the signal characteristics; this is not so for noise. Once signal and noise are separated, a new stage may be formed to further assess the network patterns of WM activity, as well as their relationships with cortical networks. This may also allow for the conjoint evaluation of the roles of WM and GM networks in perceptual, behavioral, and cognitive tasks.

Taking this strategy, we set out to characterize WM-fMRI signals in the resting state and also during free viewing of a natural movie. The natural-vision paradigm provides a dynamic and realistic behavioral context. As in the resting state, brain activity in this task state is seemingly complex and unpredictable, yet it exhibits coordinated cortical network patterns that support visual perception (Hasson et al., 2004). Here, we further asked whether the patterns of functional connectivity in the white matter would differ between the resting state and the natural-vision state. The answer to this question was expected to shed light on the functional relevance of white-matter fMRI. Briefly, high-dimensional ICA was used to decompose and de-noise WM-fMRI signals in the resting state and during a natural-vision task. From the de-noised data, we found that WM-fMRI signals were patterned into clusters and hierarchically organized in the resting state, whereas naturalistic visual stimuli drove more coherent signal fluctuations within the optic radiations, and the coupling between the WM pathways and the GM networks engaged in visual processing and perception.

Methods and Materials

Subjects

Thirteen healthy volunteers (25 ± 3 years old, 6 females, 10 right-handed, normal or corrected to normal vision) participated in this study in accordance with a protocol approved by the Institutional Review Board at Purdue University. Two subjects were excluded because they were self-reported to fall asleep during the sessions.

Experimental Design

Each subject underwent four fMRI sessions with two conditions. Two sessions were in the eyes-closed resting state, and the other two were during free-viewing of an identical movie clip (*The Good, the Bad, and the Ugly*, 1966). We chose this movie because it was previously used to obtain interesting findings on cortical gray-matter activity during natural vision (Hasson et al., 2004). Every movie-stimulation session began with a blank gray screen presented for 42 seconds, followed by the movie presented for 5 minutes and 37 seconds (from 162:54to 168:33 minutes in the film), and ended with the blank screen again for 30 seconds. No sound was played during the movie. The resting-state sessions had the same duration as the movie-stimulation sessions. The session order was randomized and counterbalanced across subjects. The scanner environment was darkened to minimize external light exposure. Hereafter, we also refer to the movie stimulation condition as the task state, in contrast to the resting state.

Data acquisition

Whole-brain structural and functional MRI images were acquired using a 3-Tesla Signa HDx MRI system (General Electric Health Care, Milwaukee, USA). A 16-channel receive-only phase array coil (NOVA Medical, Wilmington, USA) was used during all acquisitions. The fMRI data were acquired using a single-shot, gradient-recalled (GRE) echo-planar imaging (EPI) sequence (38 interleaved axial slices with 3.5 mm thickness and 3.5×3.5 mm^2 in-plane resolution, TR = 2000ms, TE = 35ms, flip angle = 78°, field of view = 22×22 cm^2). T_1-weighted anatomical images covering the whole head were acquired with a spoiled gradient recalled acquisition (SPGR) sequence ($1 \times 1 \times 1$ mm^3 nominal resolution, TR/TE = 5.7/2ms, flip angle = 12°).

Pre-processing

Pre-processing of the fMRI images was carried out with a combination of AFNI (Cox 1996), FSL (Smith et al. 2004), and MATLAB (Natick, MA). In brief, T_1-weighted anatomical images were non-linearly registered to the Montreal Neurological Institute (MNI) brain template, using a combination of *flirt* and *fnirt* in FSL. T_2*-weighted functional image time series were corrected for slice timing (using *slicetimer* in FSL), co-registered to the first volume within each series to account for head motion (using *mcflirt* in FSL), masked out non-brain tissues (using *3dAutomask* in AFNI), aligned to the T_1-weighted structural MRI (using *align_epi_anat.py* in AFNI), and registered to the MNI space with 3-mm isotropic voxels (using *applywarp* in FSL, and *3dresample* in AFNI).

The first six volumes in the fMRI data were discarded to avoid any pre-steady-state longitudinal magnetization. Each session's data was subjected to third-order de-trending and low-pass filtering (<0.1 Hz) using the regression and filtering toolboxes in MATLAB. For the movie sessions, we excluded data acquired during the blank gray screen presentation and further removed the first 6 volumes and the last 7 volumes of the movie to avoid any transient fMRI response during the movie stimulation.

Following the pre-processing steps, data analysis for the fMRI data was twofold: analysis within the WM-only and analysis within the GM-only. This was achieved by creating and applying a WM mask to the normalized fMRI images to isolate WM-only voxels. The WM mask was created from the LONI Probabilistic White Matter template in the MNI space (Shattuck et al. 2008) by setting a probabilistic threshold to a level of 0.85. This threshold was chosen to be very conservative so as to avoid possible partial volume effects close to GM/WM junctions; hence, the mask covered most but not all WM voxels. The thalamus was not included in the WM mask. The GM mask was derived by finding the intersection of the complement of the WM mask and the brain mask in the MNI template. Both the WM and GM masks were restricted to voxels within axial slices from z = −15 mm to z = 51 mm. Linear spatial smoothing (FWHM=6 mm) was then performed separately within the WM or GM voxels to avoid partial volume effects between them. Effectively, the voxels outside the mask were set to null, and thus did not contribute to the smoothed voxel intensity, while the spatially smoothed voxel time series was demeaned and variance normalized before any subsequent analysis.

De-noising via Independent Component Analysis (ICA)

For each condition (i.e. the resting state and the task state), the fMRI data were separated into two sets for each of the two sessions from every subject. In a total of four sets of fMRI data, two were from resting state and the other two from the task state with naturalistic visual stimuli. The fMRI data were then temporally concatenated across subjects for each of the sets. The four concatenated fMRI time-series data allowed us to evaluate the test-retest reproducibility of the group-level ICA maps in the resting state and the task state. Group spatial ICA using the Infomax algorithm (Bell and Sejnowski 1995) was applied to each set of the concatenated data. This gave rise to 70 spatially independent components (ICs) with distinct temporal basis functions that yielded a sparse representation of the data; as such, voxels were considered to be synchronized (i.e. functionally related) within each component. To evaluate the test-retest reproducibility of each of the 70 ICs, we calculated the spatial cross correlations between the two sets of ICs for each condition. An IC in one set was assumed to be reproducible if there was a corresponding IC in the other set that was spatially correlated with this IC. We calculated the absolute values of the correlation coefficients and found the optimal pairing by maximizing the sum of the pair-wise absolute cross-correlation values. Here, the absolute cross-correlation value was used because spatially consistent ICA components might appear 180° out of phase from one another. Upon visual inspection, non-reproducible components were regarded as noise and discarded, whereas the remaining components were re-assembled to generate the de-noised fMRI data for every session and every subject. For each condition, the de-noised fMRI data were further concatenated across the two sessions for each of the eleven subjects, giving rise to 22 sessions in total. Then, group ICA was applied again to the de-noised and concatenated data, generating about 30 ICs that characterized the WM fMRI signals in the resting state or during the natural visual stimulation.

Following group ICA, we used dual regression (Filippini et al. 2009) against each subject's fMRI data to extract subject-specific ICA maps in order to capture inter-subject differences (Tavor et al. 2016). Briefly, the first (multiple) regression applied to the spatial domain, using the group-level ICA maps as regressors to get individual time series for each subject and each component; the second regression applied to the time domain, using the obtained individual time series as regressors to get individual-level ICA maps.

Hierarchical Clustering based on Temporal Correlations

In both the resting state and the task state, the ICs of WM-fMRI signals were progressively grouped into clusters based on the cross-correlations of their corresponding time series and a complete-linkage hierarchical clustering algorithm (Dasgupta and Long 2005). At the beginning of the algorithm, each component was in a cluster of its own. These clusters were then progressively combined into larger clusters until all components ended up in the same cluster. At each step, the clusters separated by the 'shortest distance' (i.e. the largest temporal cross correlation) were combined. Such hierarchical clustering was visualized as a dendrogram, which showed the sequence of clusters merging and the distance at which each fusion took place (Cordes et al. 2002; Dasgupta and Long 2005; Wang and Li 2013).

Comparison between the Resting and Task States

We also compared the reproducibility of WM-fMRI ICA components in the resting state versus the task state. For this purpose, the test-retest reproducibility (i.e. spatial cross correlations between repeated sessions of the same condition) was compared between the resting state and the task state. Specifically, after pairing the ICA components between session 1 and session 2 of either the resting state or the task state as aforementioned, the pairwise correlation coefficients were transformed into z scores. The z scores were compared between the two states, and the significance of their differences was evaluated by using a two-sample independent t-test with the significance level at 0.05.

We further compared the WM-fMRI ICA maps in the resting state with those in the task state. Specifically, we calculated the spatial cross correlations between every component in the resting state and every component in the task state. Then, individual components in the resting state were optimally paired to those in the task state to maximize the sum of cross correlations between all paired components. After pairing, the pair-wise cross correlations were further tested for statistical significance. To calculate the p value from the correlation coefficient, we used an approximate estimate of the spatial degree of freedom (DOF), as previously described elsewhere (Smith et al., 2009). The voxels were not independent samples due to spatial smoothing. For a conservative approximation, we considered independent samples as larger (than a voxel) cubes that included five voxels in each direction, given that the voxel size is 3mm and the smoothing filter has FWHM=6 mm. For a total of 7990 voxels in WM, this approximation yielded an estimated DOF of 64. To be even more conservative, we used DOF of 50 to account for other potential spatial dependency in data acquisition or processing. Although seemingly arbitrary, the above procedure yielded a reasonable approximate of the spatial degree of the freedom.

Functional relations between WM and GM Networks

Furthermore, we assessed the functional relationships between WM and GM networks at resting or during task. For this purpose, we first identified a number of functional networks within the cortical gray matter during the resting or task state. Specifically, GM-fMRI data were concatenated across all sessions from all subjects in the resting or task state. For either state, ICA was applied to the concatenated data to produce 70 spatially independent components, among which ~45 cortical networks were recognizable as previously reported resting state networks (Shirer et al. 2012), and retained for subsequent analyses.

We evaluated the temporal cross correlations between ICA components in WM and those in GM. The activity time series of every WM and GM component was extracted from each of the 22 sessions separately for the resting state and the task state. For every session of the resting or task state, temporal cross correlations were calculated between every GM component and every WM component, and then transformed to z scores. To test the significance of the cross correlation, the average z score was compared against zero by performing one-sample t-test to every pair of GM and WM components ($p<0.05$, DOF=21).

Comparison with diffusion MRI

For both resting-state and task conditions, we thresholded the spatial ICA maps to delineate the shapes of WM structures revealed in individual components using the method described in Beckmann and Smith 2004. Briefly, we first calculated the z-statistic for each voxel and each ICA map by dividing the ICA maps by the estimated standard deviations of the voxel-wise residuals. We further modeled the null distribution of each z-statistic map with a mixture of two Gaussian distributions (i.e. Gaussian Mixture Model (GMM)), and then calculated the voxel-wise posterior probability based on the estimated GMM. We then thresholded the ICA maps according to the voxel-wise posterior probability, which was set to 0.6.

For each condition, we then used the thresholded ICA maps to create a set of WM structures. Such structures, obtained with WM-fMRI in the resting or task state, were visualized in the open-source 3D Slicer toolkit (http://www.slicer.org) (Fedorov et al. 2012), and were compared with a diffusion tensor imaging atlas, the ICBM-DTI-81 white-matter labels atlas (Mori et al. 2008; Oishi et al. 2008).

Results

Spatially independent components of resting-state WM fMRI signals

We explored the spatiotemporal patterns of WM-fMRI data in the resting state by using ICA. 70 spatially independent components were extracted from all WM voxel time series, after data were temporally standardized and concatenated across all subjects and separately for the two repeated resting-state sessions (referred to as session 1 & session 2). Components from the two sessions were optimally matched into distinct pairs based on the spatial cross correlation between each component from session 1 and its corresponding component from session 2. This pair-wise cross-correlation provided the measure of intra-subject reproducibility for each component. Twenty-eight out of the 70 components were found to exhibit relatively high intra-subject reproducibility ($|r|=0.4028 \pm 0.0276$) and were paired between the two repeated sessions. Fig. 1 shows the spatial patterns of five example components that were found to be reproducible between session 1 (Fig. 1, left) and session 2 (Fig. 1, middle). Many of the reproducible components appeared cluster-like (or non-fiber-like), showing spatial distributions confined to focal regions in WM (e.g. Fig. 1 IC 1 and IC 6). In contrast, some components were readily observed as a fiber-like distribution over a long distance, as in the optic radiations (e.g. Fig. 1, IC 2 and IC 13), and the corpus callosum (e.g. Fig. 1 IC 8).

We discarded those “noise” components that were spatially inconsistent between the two repeated sessions in order to improve the SNR of WM-fMRI data. The discarded components had either relatively lower reproducibility ($|r|=0.1879 \pm 0.0147$) between session 1 and session 2, or spatially non-specific distribution most likely due to artifacts. Thus, we attributed the 28 reproducible components to the “signals” likely of neural origin, and attributed the 42 non-reproducible components to “noise”. Such “signal” vs. “noise” components accounted for 33.98% and 66.02% of the variance in WM-fMRI, respectively.

After excluding all noise/artifact components, the signal components were reassembled to give rise to presumably de-noised WM-fMRI data. The de-noised data were then concatenated across the two resting-state sessions, and further decomposed into 31 spatially independent components for subsequent analyses. Here, a buffer (+3 ICs) was provided to account for the variation between the two sessions. Among the 31 components, two components were not consistent to the spatial maps produced by ICA in either session 1 or session 2; they were further discarded, leaving a total of 29 components for subsequent analyses. Some example components extracted from the de-noised data are shown in Fig. 1 (right). All of the 29 components in the resting state are shown in Fig. 2.A.

Hierarchical Organization of WM-fMRI components

We assessed the temporal relationships between different components of the de-noised WM-fMRI data. These components, although spatially independent, were temporally correlated with each other to a varying degree, with the absolute correlation coefficients ranging from 0.00 to 0.27 (Fig. 2.B, bottom). These temporal cross-correlations were used to progressively merge the individual components into a hierarchical organization based on hierarchical clustering (Fig. 2.B, top). For example, bilateral optic radiations emerged from progressively merging multiple ICs: two adjacent ICs were first grouped into a unilateral fiber bundle connecting LGN to V1, and then it was paired with the homologous fiber bundle from the opposite hemisphere (Fig. 2.C). Similarly, adjacent segments in the corona radiata (Fig. 2.A – IC 17 and IC 28) were clustered to construct the overall fiber bundle (Fig. 2.B). For comparison, we also applied the same hierarchical clustering analysis to cortical networks. Results showed that cortical networks were more tightly correlated and clustered than white-matter components (Fig. S1).

Spatiotemporal Structure of WM-fMRI during natural vision

Following this result, we asked whether the above intrinsic patterns and the hierarchical structure of WM-fMRI signals were preserved during complex, dynamic and realistic visual experiences. To address this question, we analyzed the WM-fMRI data during naturalistic visual stimulation using the same method applied in the resting state. Similar to the test-retest reproducibility evaluated for the resting-state components (Fig. 3.A, left), some ICA components were reproducible across the two repeated movie stimulation sessions (Fig. 3.A, middle). Twenty-seven components were reproducible ($|r|=0.5867 \pm 0.0323$) and were kept as signals, while other components was attributed to noise or artifacts and thus removed. The signal and noise/artifact components accounted for 34.69% and 65.31% of the variance in WM-fMRI, respectively, which was comparable to that of those in the resting state. Overall, the components during the visual task were more reproducible than those in the resting state (Fig. 3.A, right) ($p<0.0001$, two-sample t-test). As done for the resting state, we also concatenated the de-noised WM-fMRI data across the two movie sessions, and decomposed the concatenated data into 30 spatially independent components. Two components were not consistent with any of the components produced by ICA in either session 1 or session 2; the other 28 components were kept for subsequent analyses.

The task-state WM ICs mostly resembled those in the resting state (Fig. 3.B). Twenty-one out of the 28 components observed during the visual task were also observed in the resting

state, giving rise to one-to-one matched pairs with significantly correlated spatial patterns ($|r| = 0.5306 \pm 0.0298$, $p < 10^{-5}$ to $p = 0.0207$, uncorrected, paired IC 1 (rest) and IC 14 (task) were slightly above this threshold with $p = 0.0710$). For example, IC 3, IC 10, IC 27 were three ICA maps in the task state that were matched to IC 8, IC 14, IC 6 in the resting state (Fig. 3.B). Four components were not matched ($|r| = 0.0868 \pm 0.0182$, $p = 0.3208$ to $p = 0.8611$, uncorrected) in a one-to-one manner. For an example, see Fig. 3.B, IC 1.

To further characterize the consistency (and inconsistency) between the resting and task states, we compared the hierarchical relationships between spatially independent components in these two states. See Fig. 4.A for all 28 components in the task state. The independent components that were matched between the task and resting states were also found to bear a similar hierarchical organization in both states (Fig. 4.D). For example, the corona radiata began to emerge from clustering its three segments (IC 8, IC 23, and IC 17) through two hierarchical steps (Fig. 4.B). Among the components that were not matched between the task and resting states, a single component (IC 1) in the task state was found to encompass the bilateral optic radiations connecting LGN and V1 (Fig. 4.C). This observation that the bilateral optic radiations manifested themselves as a single component suggests that activity fluctuations within the optic radiations were more coherent during the visual stimulation than in the resting state, during which the optic radiations were segregated into multiple pieces (Fig. 2.C). Also note that during the task, the optic radiations (IC 1) were further clustered with a component corresponding to an anterior segment in the right inferior longitudinal fascicular (ILF) (IC 13), which is located near and posterior to the optic radiations (see Fig. 4.A & Fig. 4.D) and contains connections between associative visual areas and anterior temporal structures (Catani et al. 2003).

While the above results were obtained with group ICA, we also used dual regression to obtain the corresponding ICA maps from individual subjects. For both the resting state and the task state, the individual-level ICA maps were generally consistent with the group-level ICA maps (Fig. 5).

Interactions between WM and GM Networks

To further explore the functional role of the coherent signal within the optic radiations, we evaluated its coupling with cortical visual networks in GM by computing their temporal cross correlations. For this purpose, 70 spatially independent components were extracted from all GM voxel time series after concatenating every session and every subject for the visual task; among those, 47 components were recognizable as established intrinsic functional networks (Shirer et al. 2012). We identified four cortical networks that had the highest (and significant) positive cross-correlations with the optic radiations ($p = 0.01$ to 0.047, one-sample t-test, uncorrected). As shown in Fig. 6A, all of these four networks were parts of the visual system: namely, the primary visual area (IC 4), higher order visual networks (IC 1 and IC 3), and a medial visual network (IC 2). These areas are involved in natural visual processing, as shown in previous studies (Hasson et al. 2004).

We performed this analysis on the resting-state data to assess the temporal relationships between the optic radiations and intrinsic visual networks in the absence of the visual task. As shown in Fig. S2, we identified four cortical networks in the resting state as the

counterparts to those vision-related components shown in Fig. 6.A. The optic radiations resting-state component was formed from a sum of the three optic radiations components (IC 11, IC 13, and IC 2) shown in Fig. 2.C; the time series was formed from the mean of those of the three components. However, unlike the task state (Fig. 6.B, left), the resting state did not exhibit any significant temporal cross correlations between the optical radiations and resting-state visual networks ($p = 0.1003$ to 0.9526, uncorrected) (Fig. 6.B, right).

However, head motion was a potential confounding factor to the above findings. We found that the head motion parameters (translations and rotations) exhibited on average 2.3 and 3.5 times greater standard deviations in the resting state than in the task state, respectively. This difference was significant ($p<0.00001$, Wilcoxon rank sum test). Despite the significantly different head motion between the two states, this difference was less likely to account for the spatially and functionally specific findings about WM components and their interactions with GM networks, the time courses of which did not show the slow drift or abrupt changes that characterized the head motion. In addition, we were concerned about whether head movements in the task condition were task related; i.e. that common movements between sessions would occur at particular moments in the movie at particularly suspenseful or surprising points. To effectively capture sudden movements while ignoring slow drifts, we evaluated the time derivative of every motion-correction parameter and calculated its correlation between the repeated movie sessions within each subject. Only marginal correlation was found ($r<0.08$) for all six motion parameters. Therefore, head motion was a confound of major concern.

Relationships with white-matter structure

Finally, we asked whether the ICA maps obtained with WM-fMRI in the resting state and the task state were distributed along the axonal fiber tracts. For this purpose, we compared the thresholded ICA maps with white-matter tracts based on diffusion MRI using the ICBM-DTI-81 white-matter labels atlas (Mori et al. 2008; Oishi et al. 2008) (Fig. 7). Qualitatively, for both the resting and task states, most of the ICA components of WM-fMRI data covered only segments of individual fiber tracts, without extending the full tract length. However, some components appeared to align well with major fiber bundles (e.g. the optic radiations, the corpus callosum, and the internal capsule). It suggests a complex structure-function relationship in the white matter, when observed with white-matter diffusion and functional MRI.

Discussion

Using data-driven analysis methods, we examined the spatiotemporal characteristics of fMRI time series in the cerebral white matter both in the resting state and during naturalistic visual perception. Results led to the following findings: 1) spatially independent components of resting-state fMRI signals in WM revealed reproducible cluster-like or fiber-like structures with synchronized spontaneous fluctuations within each structure; 2) different components were temporally correlated in a hierarchical manner, leading us to report the intrinsic functional organization of WM fiber tracts; 3) such intrinsic structures and their

hierarchical organization were mostly preserved during naturalistic visual stimulation; 4) however, a subset of these structures that were engaged in visual processing showed stronger synchronization within themselves and significant interactions with cortical visual networks. Therefore, fMRI signals in WM, like those in GM, may be utilized to uncover the intrinsic functional organization of WM, and to map axonal pathways that support neural signaling between cortical networks during complex tasks. The WM-fMRI methods as reported here and elsewhere (e.g. Gawryluk et al., 2014; Ding et al., 2016), as well as functional DTI methods (Mandl et al. 2008; Spees et al. 2013), may begin to uncover WM functionality in health and disease.

Spontaneous WM-fMRI signals reflect the hierarchical organization of axonal fibers

Spatial ICA has been widely used to map large-scale resting state networks (RSN) (Beckmann and Smith 2004; Calhoun et al. 2008), especially when one seeks a relatively lower number of components. For a large-scale RSN that typically includes multiple discrete GM regions (e.g. the default-mode network), those regions are temporally correlated (Van Dijk et al. 2010) and structurally inter-connected through axonal fibers (Greicius et al. 2009). In other words, such large-scale RSNs have corresponding structural substrates to support neural signaling between different GM regions in the RSN (van den Heuvel and Sporns 2013). It is thus tempting to hypothesize that the WM substrate underlying a GM network carries synchronized activity within itself, whereas the WM substrates underlying different GM networks are temporally distinct in order to support their different functions. If this hypothesis were true, one would expect to be able to use ICA to decompose resting-state WM-fMRI signals into spatially independent and temporally distinct WM sub-systems that consist of axonal fibers connecting regions comprising individual GM networks.

However, spatially independent components of resting-state WM-fMRI signals did not appear as long-range fiber tracts; instead, they were mostly shown as cluster-like (or non-fiber-like) patterns, appearing as local segments of fiber tracts with a varying length. Nevertheless, these seemingly fragmented components were not isolated to each other, but exhibited a varying level of temporal cross correlations. These fragments tended to be more correlated if they were parts of the same fiber tract; combining these correlated components gave rise to the entire fiber tract; the combined fiber tract on one hemisphere tended to be correlated with the homologous fiber tract in the opposite hemisphere. As such, functional networks of WM fiber tracts did not readily result from a single-level decomposition of the WM-fMRI signals; instead, they emerged progressively as short segments of fiber tracts were combined into a hierarchical organization based on their temporal relations.

The cluster-like appearance and hierarchical organization of the WM-fMRI ICA components might be counter-intuitive given what is known about neuronal structure. While the dendrites and the soma of a neuron occupy a tiny volume in GM, its axon runs a long distance in WM for relaying neuronal spikes. Different locations along the axon carry the same functional information, and thus are expected to be temporally synchronized along a long and continuous pathway in the fMRI time scale. However, the spatial resolution of fMRI is insufficient to resolve axons. An fMRI voxel samples a cubic piece of a large axonal bundle, containing a mixture of neuronal activity along every axon in the bundle. The fact that axons

are routed and bundled differently at different voxels is expected to cause discontinuity in the spatial patterns of temporal synchronization in the fMRI signal. We speculate that this discontinuity is a major reason why ICA applied to coarsely sampled WM-fMRI data tend to reveal segments of fiber tracts as opposed to the intact long-range fiber tracts.

Also contributing to the discontinuity and segregation of the WM-fMRI signal is the orientation-dependence of T_2*-sensitive MRI in WM. Magnetic susceptibility contrast in WM is anisotropic due to the highly oriented water compartments of the axonal bundles (Lee et al. 2011; Duyn 2013). This may in part explain why regions with higher densities of parallel axons, such as the corpus callosum, are more reliably detected in previous WM-fMRI activation studies. Interestingly, Ding et al. showed that the tensor of local temporal correlations in WM-fMRI signals demonstrated similar orientations as those observed with diffusion MRI (Ding et al. 2013), and could be specifically altered by tasks (Ding et al. 2016). Combining local and global correlation structures of WM-fMRI is a potentially promising direction for future studies.

Natural-vision task reshapes the WM functional organization

It has been increasingly recognized that spontaneously emerging network patterns are functionally significant since such activity patterns are well preserved from the resting state to various task states (Kenet et al. 2003; Smith et al. 2009; Wilf et al. 2015). Findings from the present study further extend this conclusion from the gray matter to the white matter. During naturalistic visual stimulation, the WM-fMRI signals exhibited reproducible independent components with similar spatial distributions as those observed in the resting state. Therefore, like those in the cortex, resting-state fMRI patterns within WM also reflect intrinsic functional units that are recruited to perform complex tasks. Although intrinsic functional structures in WM were preserved during the naturalistic visual task, the task enhanced the temporal synchronization within the task-related WM structures, as well as between the task-related WM structures and GM networks. The former is supported by the finding that bilateral visual pathways emerge as a single component, as opposed to the multiple hierarchical components found during the resting state; this implies that a stronger level of synchronization between the left and right optic radiations occur along with the tract emanating from LGN. The latter is supported by the finding that the WM component showing optic radiations is significantly correlated with several cortical visual networks during the task, but not during resting-state (also discussed later).

Previous studies have shown that natural vision evokes reliable cortical fMRI responses (Hasson et al. 2004; Jääskeläinen et al. 2008) and spiking activity (Belitski et al. 2008; McMahon et al. 2015) within and across subjects. Interestingly, Mukamel et al. have shown significant correlations between spiking activity and fMRI response between different subjects watching the same movie (Mukamel et al. 2005). Furthermore, Astafiev et al. have demonstrated a link between BOLD fMRI in the MT+/LO and FA (measured through DTI) in the left optic radiation in mTBI patients (Astafiev et al. 2016). Extrapolating these studies and the findings from this study, we speculate that natural visual perception induces reliable and synchronized WM activity, which gives rise to spiking activity as the direct effect, and the fMRI signal as the secondary indirect effect. While this speculation is reasonable, it

remains to be confirmed, ideally with simultaneous white-matter neural recording and fMRI imaging.

Biophysical and physiological origins of WM-fMRI

Here, the so-called "fMRI" signal refers to the temporal variation of voxel intensity in gradient-echo echo-planar imaging (GE-EPI) images that primarily carry the T_2*-weighted contrast. Multiple sources contribute to this signal, but those sources may or may not bear any relationship to underlying neural activity (Bianciardi et al. 2009). For the signals from gray-matter voxels, the source related to neural activity is blood oxygenation level dependent (BOLD) (Ogawa et al. 1990). The BOLD fluctuation reflects the combined effects of cerebral blood flow (CBF), blood volume (CBV), and the metabolic rate of oxygen ($CMRO_2$) (Buxton et al. 1998). Such hemodynamic and metabolic changes are coupled to neural activity in terms of both synaptic input and spiking output (Logothetis et al. 2001; Smith et al. 2002). While the basis of fMRI is complex, as it is a topic of active research and debate (Leopold and Maier 2012), extra caution should be exercised when interpreting WM-fMRI.

Is the WM-fMRI signal BOLD? Despite a lower density of vasculature, the white matter has the vascular capacity for MRI-detectable hemodynamic changes (Gawryluk et al. 2014). Two defining features of the BOLD mechanism, cerebrovascular reactivity (Ogawa et al. 1990) and echo-time dependence (Kundu et al. 2012), have been both demonstrated for the WM-fMRI signal. The WM vasculature dilates in response to hypercapnia, showing detectable CBF and BOLD responses in the white matter, although the responses have a lower magnitude than in the gray matter (Rostrup et al. 2000; Thomas et al. 2014). The fluctuation and correlation of WM-fMRI signals at rest vary with different echo times, reaching their maxima at a similar echo time as the T_2* in the gray matter (Ding et al. 2016). In addition, metabolic changes to neuromodulation are observable in the white matter (Weber et al. 2002). Astrocytes, which mediate neurovascular coupling in gray matter (Petzold and Murthy 2011), are also present in white matter (Waxman and Ritchie 1993; Rash 2010). Therefore, all of the necessary machinery for neurometabolic and neurovascular coupling, are generally in place in the white matter to give rise to detectable BOLD signals.

If it is BOLD, does the WM-fMRI signal report neural activity? WM-fMRI signals show task-dependent activations as reviewed in (Gawryluk et al. 2014). Their correlational structures are reorganized from the resting state to the task state, as shown in this study, as well as in (Ding et al. 2016). Therefore, the WM-fMRI signals are functionally relevant, and hence report, at least in part, neural activity in the white matter. However, it is not trivial and largely speculative to posit the specific type of neural activity that is coupled with the WM-fMRI signal. The BOLD signal is an indirect measure of neural activity (Logothetis and Wandell 2004). In the gray matter, the neuronal origin of the BOLD signal may be synaptic activity observed with local field potential (Logothetis et al. 2001; Viswanathan and Freeman 2007), or spiking activity observed with single or multi-unit activity (Smith et al. 2002; Mukamel et al. 2005). Synaptic activity (neuronal input) and spiking activity (neuronal output) are inherently linked with one another most of the time; their individual couplings with the BOLD signal are in fact comparable (Logothetis et al. 2001). When they

have been dissociated under special experimental conditions, the BOLD signal has been found to be more coupled with synaptic activity (Viswanathan and Freeman 2007; Rauch et al. 2008), although counter-examples have also been demonstrated (Pelled et al. 2009). As such, it is still not quantitatively understood which specific types of neuronal activity drive BOLD-fMRI. It is at least plausible that spiking activity is partly coupled with the BOLD signal, even in the gray matter. In the white matter, neuronal activity is mostly spiking activity propagating along the axon, with little synaptic activity (Gawryluk et al., 2014). This leads us to hypothesize that the WM-fMRI signal is BOLD and indirectly coupled to spiking activity. Nevertheless, this hypothesis is speculative and remains to be tested, while the signaling pathway that potentially links spiking activity to vasodilation also needs to be elucidated. To the best of our knowledge, there is no study directly addressing the relationship between spiking and fMRI signals in the white matter.

Methodological considerations

We did not observe significant interactions between WM and GM at rest, but during task (Fig. 6.B). A possible explanation for this observation was that the task might drive greater WM activity fluctuations, and thus a higher SNR. We did not expect the difference in SNR as a major contributor, because the fraction of the data variance explained by the signal versus noise components was comparable for the task state and the resting state. Given future improvement in the SNR of WM-fMRI, we anticipate that significant WM-GM correlations may also be observable even at rest, while tasks would further strengthen such correlations.

As mentioned in Introduction, the separation of the WM voxels from the GM voxels is an essential preprocessing step in this work, in order to deal with the different dynamic range and correlational structure in WM and GM. When we performed a whole-brain ICA analysis on resting state fMRI data without WM-GM separation (the number components was 70), most of the components were gray-matter networks, as previously shown in numerous resting state fMRI studies. There were a few components for which the spatial distributions were more in the white matter than in the gray matter, as shown in Fig. S4. Given the very small number of white-matter-like components, the components tended to capture the patterns with the strongest degree of coherence (e.g. the global white-matter pattern, the optic radiations, and the corpus callosum). Such a whole-brain analysis did not allow for finer-grained pattern analysis and hierarchical clustering in the white matter, as enabled by only looking at the white-matter voxels.

Spatial smoothing was also helpful to improve the SNR of WM-fMRI. When we performed the white-matter ICA analysis on data without spatial smoothing, some of the general features are still observed, even without smoothing (Fig. S3). However, without spatial smoothing, the overall reproducibility of the ICA maps was lower (Fig. S3.A). Given the same criteria of selecting signal versus noise ICA components, we were only able to identify less than 10 “signal” components in the white matter, making the denoising process more challenging. However, when we kept an identical number of components, we found qualitatively similar results in that components showing optic tracts appeared unilateral in

the resting state (Fig. S3.B), but bilateral in the task state (Fig. S3.C). Thus, the spatial smoothing is a helpful preprocessing step but not as essential as is the WM-GM separation.

Head motion is generally a concern in fMRI (Van Dijk et al. 2012) and is likely a confounding factor in our WM-fMRI findings. In this study, we found that the resting state sessions had significantly more head motion than the task state, likely because the engagement in the natural movie helped the subjects restrain their heads. Although we could not rule out the potential effects of head motion, we considered it as a minor confound to the WM-fMRI signals and components for the following reasons. First, the effects of head motion usually occur at the borders of different tissues (e.g. GM versus WM). As mentioned before, we used a conservative WM mask so as to avoid voxels around the GM-WM borders. Second, most of the head motion parameters varied in time as slow drifts, which were discounted as the WM-fMRI signals were detrended (by removing up to 3rd order polynomial functions). Furthermore, the ICs kept in the ICA-based denoising procedure were consistent across sessions and subjects, unlikely to be attributable to head motions. The time courses of the “signal” components also did not show either any signal drift or any abrupt change, which likely arose from head motion. Finally, it is worth noting that overall, our results demonstrate that head movements occurring during the task are unlikely to be task-related.

Supplementary Material

Refer to Web version on PubMed Central for supplementary material.

Acknowledgments

The research was supported in part by NIH R01MH104402 (Z Liu, PI), and a predoctoral fellowship to Lauren Marussich as supported by TL1 TR001107 and UL1 TR001108 (A. Shekhar, PI) from the National Institutes of Health, National Center for Advancing Translational Sciences, Clinical and Translational Sciences Award. The authors would also like to thank Yu Tang for her assistance with data analysis during the exploratory phase of this project.

References

Astafiev SV, Shulman GL, Metcalf NV, Rengachary J, MacDonald CL, Harrington DL, Maruta J, Shimony JS, Ghajar J, Diwakar M, et al. Abnormal White Matter Blood-Oxygen-Level-Dependent Signals in Chronic Mild Traumatic Brain Injury. J. Neurotrauma. 2015; 32:1254–1271. [PubMed: 25758167]

Astafiev SV, Zinn KL, Shulman GL, Corbetta M. Exploring the physiological correlates of chronic mild traumatic brain injury symptoms. NeuroImage Clin. 2016; 11:10–19. [PubMed: 26909324]

Bandettini, Pa, Wong, EC., Hinks, RS., Tikofsky, RS., Hyde, JS. Time course EPI of human brain function during task activation. Magn. Reson. Med. 1992; 25:390–397. [PubMed: 1614324]

Beckmann CF, Smith SM. Probabilistic Independent Component Analysis for Functional Magnetic Resonance Imaging. IEEE Trans. Med. Imaging. 2004; 23:137–152. [PubMed: 14964560]

Belitski, a, Gretton, a, Magri, C., Murayama, Y., Montemurro, M., Logothetis, N., Panzeri, S. Local Field Potentials and Spiking Activity in Primary Visual Cortex Convey Independent Information about Natural Stimuli. J. Neurosci. 2008; 28:5696–5709. [PubMed: 18509031]

Bell, aJ, Sejnowski, TJ. An information-maximization approach to blind separation and blind deconvolution. Neural Comput. 1995; 7:1129–1159. [PubMed: 7584893]

Bianciardi M, Fukunaga M, van Gelderen P, Horovitz SG, de Zwart JA, Shmueli K, Duyn JH. Sources of functional magnetic resonance imaging signal fluctuations in the human brain at rest: a 7 T study. Magn. Reson. Imaging. 2009; 27:1019–1029. [PubMed: 19375260]

Biswal B, Yetkin FZ, Haughton VM, Hyde JS. Functional connectivity in the motor cortex of resting human brain using echo-planar MRI. Magn. Reson. Med. 1995; 34:537–541. [PubMed: 8524021]

Buxton RB, Wong EC, Frank LR. Dynamics of blood flow and oxygenation changes during brain activation: the ballon model. Magn Reson Med. 1998; 39:855–864. [PubMed: 9621908]

Calhoun VD, Kiehl KA, Pearlson GD. Modulation of temporally coherent brain networks estimated using ICA at rest and during cognitive tasks. Hum. Brain Mapp. 2008; 29:828–838. [PubMed: 18438867]

Catani M, Jones DK, Donato R, Ffytche DH. Occipito-temporal connections in the human brain. Brain. 2003; 126:2093–2107. [PubMed: 12821517]

Cordes D, Haughton V, Carew JD, Arfanakis K, Maravilla K. Hierarchical clustering to measure connectivity in fMRI resting-state data. Magn. Reson. Imaging. 2002; 20:305–317. [PubMed: 12165349]

Cox RW. AFNI: Software for Analysis and Visualization of Functional Magnetic Resonance Neuroimages. Comput. Biomed. Res. 1996; 29:162–173. [PubMed: 8812068]

Dasgupta S, Long PM. Performance guarantees for hierarchical clustering. J. Comput. Syst. Sci. 2005; 70:555–569.

Van Dijk, KRa, Hedden, T., Venkataraman, A., Evans, KC., Lazar, SW., Buckner, RL. Intrinsic functional connectivity as a tool for human connectomics: theory, properties, and optimization. J. Neurophysiol. 2010; 103:297–321. [PubMed: 19889849]

Van Dijk KRA, Sabuncu MR, Buckner RL. The Influence of Head Motion on Intrinsic Functional Connectivity MRI. Neuroimage. 2012; 59:431–438. [PubMed: 21810475]

Ding Z, Newton AT, Xu R, Anderson AW, Morgan VL, Gore JC. Spatio-temporal correlation tensors reveal functional structure in human brain. PLoS One. 2013; 8

Ding Z, Xu R, Bailey SK, Wu T-L, Morgan VL, Cutting LE, Anderson AW, Gore JC. Visualizing functional pathways in the human brain using correlation tensors and magnetic resonance imaging. Magn. Reson. Imaging. 2016; 34:8–17. [PubMed: 26477562]

Duyn J. MR susceptibility imaging. J. Magn. Reson. 2013; 229:198–207. [PubMed: 23273840]

Fabri M, Polonara G, Mascioli G, Salvolini U, Manzoni T. Topographical organization of human corpus callosum: An fMRI mapping study. Brain Res. 2011; 1370:99–111. [PubMed: 21081115]

Fedorov A, Beichel R, Kalpathy-Cramer J, Finet J, Fillion-Robin JC, Pujol S, Bauer C, Jennings D, Fennessy F, Sonka M, et al. 3D Slicer as an image computing platform for the Quantitative Imaging Network. Magn. Reson. Imaging. 2012; 30:1323–1341. [PubMed: 22770690]

Ffytche DH, Catani M. Beyond localization: from hodology to function. Philos. TransR. Soc. LondB. Biol. Sci. 2005; 360:767–779.

Filippini N, MacIntosh BJ, Hough MG, Goodwin GM, Frisoni GB, Smith SM, Matthews PM, Beckmann CF, Mackay CE. Distinct patterns of brain activity in young carriers of the APOE-epsilon4 allele. Pnas. 2009; 106:7209–7214. [PubMed: 19357304]

Fox MD, Raichle ME. Spontaneous fluctuations in brain activity observed with functional magnetic resonance imaging. Nat Rev Neurosci. 2007; 8:700–711. [PubMed: 17704812]

Gawryluk JR, Mazerolle EL, Brewer KD, Beyea SD, D'Arcy RCN. Investigation of fMRI activation in the internal capsule. BMC Neurosci. 2011; 12:56. [PubMed: 21672250]

Gawryluk JR, Mazerolle EL, D'Arcy RCN. Does functional MRI detect activation in white matter? A review of emerging evidence, issues, and future directions. Front. Neurosci. 2014; 8:1–12. [PubMed: 24478622]

Greicius MD, Supekar K, Menon V, Dougherty RF. Resting-state functional connectivity reflects structural connectivity in the default mode network. Cereb. Cortex. 2009; 19:72–78. [PubMed: 18403396]

Harris JJ, Attwell D. The energetics of central nervous system white matter. J. Neurosci. 2012; 32:356–371. [PubMed: 22219296]

Hasson U, Nir Y, Levy I, Fuhrmann G, Malach R. Intersubject synchronization of cortical activity during natural vision. Science. 2004; 303:1634–1640. [PubMed: 15016991]

van den Heuvel MP, Sporns O. An Anatomical Substrate for Integration among Functional Networks in Human Cortex. J. Neurosci. 2013; 33:14489–14500. [PubMed: 24005300]

Jääskeläinen IP, Koskentalo K, Balk MH, Autti T, Kauramäki J, Pomren C, Sams M. Inter-subject synchronization of prefrontal cortex hemodynamic activity during natural viewing. Open Neuroimag. J. 2008; 2:14–19. [PubMed: 19018313]

Jensen JH, Lu H, Inglese M. Microvessel density estimation in the human brain by means of dynamic contrast-enhanced echo-planar imaging. Magn. Reson. Med. 2006; 56:1145–1150. [PubMed: 17029231]

Jo HJ, Saad ZS, Simmons WK, Milbury La, Cox RW. Mapping sources of correlation in resting state FMRI, with artifact detection and removal. Neuroimage. 2010; 52:571–582. [PubMed: 20420926]

Johnstone T, Ores Walsh KS, Greischar LL, Alexander AL, Fox AS, Davidson RJ, Oakes TR. Motion correction and the use of motion covariates in multiple-subject fMRI analysis. Hum. Brain Mapp. 2006; 27:779–788. [PubMed: 16456818]

Kenet T, Bibitchkov D, Tsodyks M, Grinvald A, Arieli A. Spontaneously emerging cortical representations of visual attributes. Nature. 2003; 425:954–956. [PubMed: 14586468]

Kundu P, Inati SJ, Evans JW, Luh W-M, Bandettini PA. Differentiating BOLD and non-BOLD signals in fMRI time series using multi-echo EPI. Neuroimage. 2012; 60:1759–1770. [PubMed: 22209809]

Kwong KK, Belliveau JW, Chesler DA, Goldberg IE, Robert M, Poncelet BP, Kennedy DN, Hoppel BE, Cohen MS, Cheng H, et al. Dynamic Magnetic Resonance Imaging of Human Brain Activity During Primary Sensory Stimulation Source. Proceedings of the National Academy of Sciences of the United States of America. 1992; 89:5675–5679. Vol Published by: National Academy of Sciences Stable URL: http://. Proc. Natl. Acad. Sci. U. S. A. [PubMed: 1608978]

Lee J, van Gelderen P, Kuo LW, Merkle H, Silva AC, Duyn JH. T2*-based fiber orientation mapping. Neuroimage. 2011; 57:225–234. [PubMed: 21549203]

Leopold DA, Maier A. Ongoing physiological processes in the cerebral cortex. Neuroimage. 2012; 62:2190–2200. [PubMed: 22040739]

Lierse W, Horstmann E. Anatomy of the Cerebral Vascular Bed with Special Emphasis on Homogeneity and Inhomogeneity in Small Parts of the Gray and White Matter. Acta Neurol. Scand. 1965; S14:15–19.

Logothetis NK, Pauls J, Augath M, Trinath T, Oeltermann a. Neurophysiological investigation of the basis of the fMRI signal. Nature. 2001; 412:150–157. [PubMed: 11449264]

Logothetis NK, Wandell Ba. Interpreting the BOLD signal. Annu. Rev. Physiol. 2004; 66:735–769. [PubMed: 14977420]

Makedonov I, Chen JJ, Masellis M, MacIntosh BJ. Physiological fluctuations in white matter are increased in Alzheimer's disease and correlate with neuroimaging and cognitive biomarkers. Neurobiol. Aging. 2015; 37:12–18. [PubMed: 26476600]

Mandl RCW, Schnack HG, Zwiers MP, van der Schaaf A, Kahn RS, Hulshoff Pol HE. Functional diffusion tensor imaging: Measuring task-related fractional anisotropy changes in the human brain along white matter tracts. PLoS One. 2008; 3

Mazerolle EL, Beyea SD, Gawryluk JR, Brewer KD, Bowen CV, D'Arcy RCN. Confirming white matter fMRI activation in the corpus callosum: Co-localization with DTI tractography. Neuroimage. 2010; 50:616–621. [PubMed: 20053383]

Mazerolle EL, Gawryluk JR, Dillen KNH, Patterson Sa, Feindel KW, Beyea SD, Stevens M, Tynan R, Newman AJ, Schmidt MH, et al. Sensitivity to White Matter fMRI Activation Increases with Field Strength. PLoS One. 2013; 8:1–12.

McMahon DBT, Russ BE, Elnaiem HD, Kurnikova aI, Leopold Da. Single-Unit Activity during Natural Vision: Diversity, Consistency, and Spatial Sensitivity among AF Face Patch Neurons. J. Neurosci. 2015; 35:5537–5548. [PubMed: 25855170]

Mori S, Oishi K, Jiang H, Jiang L, Li X, Akhter K, Hua K, Faria AV, Mahmood A, Woods R, et al. Stereotaxic white matter atlas based on diffusion tensor imaging in an ICBM template. Neuroimage. 2008; 40:570–582. [PubMed: 18255316]

Mosier KM, Liu W, Maldjian Ja, Shah R, Modi B. Lateralization of Cortical Function in Swallowing: A Functional MR Imaging Study. Am. J. Neuroradiol. 1999; 20:1520–1526. [PubMed: 10512240]

Mukamel R, Gelbard H, Arieli A, Hasson U, Fried I, Malach R. Coupling Between Neuronal Firing, Field Potentials, and fMRI in Human Auditory Cortex. Science (80-.). 2005; 309:951–954.

Ogawa S, Lee TM, Kay AR, Tank DW. Brain magnetic resonance imaging with contrast dependent on blood oxygenation. Proc. Natl. Acad. Sci.U. S. A. 1990; 87:9868–9872. [PubMed: 2124706]

Ogawa S, Tank DW, Menon R, Ellermann JM, Kim SG, Merkle H, Ugurbil K. Intrinsic signal changes accompanying sensory stimulation: functional brain mapping with magnetic resonance imaging. Proc. Natl. Acad. Sci. U. S. A. 1992; 89:5951–5955. [PubMed: 1631079]

Oishi K, Zilles K, Amunts K, Faria A, Jiang H, Li X, Akhter K, Hua K, Woods R, Toga AW, et al. Human brain white matter atlas: Identification and assignment of common anatomical structures in superficial white matter. Neuroimage. 2008; 43:447–457. [PubMed: 18692144]

Van Osch MJP, Teeuwisse WM, Van Walderveen Maa, Hendrikse J, Kies Da, Van Buchem Ma. Can arterial spin labeling detect white matter perfusion signal? Magn. Reson. Med. 2009; 62:165–173. [PubMed: 19365865]

Pelled G, Bergstrom Da, Tierney PL, Conroy RS, Chuang K-H, Yu D, Leopold Da, Walters JR, Koretsky AP. Ipsilateral cortical fMRI responses after peripheral nerve damage in rats reflect increased interneuron activity. Proc. Natl. Acad. Sci. U. S. A. 2009; 106:14114–14119. [PubMed: 19666522]

Petzold GC, Murthy VN. Role of astrocytes in neurovascular coupling. Neuron. 2011; 71:782–796. [PubMed: 21903073]

Rash JE. Molecular disruptions of the panglial syncytium block potassium siphoning and axonal saltatory conduction: pertinence to neuromyelitis optica and other demyelinating diseases of the central nervous system. Neuroscience. 2010; 168:982–1008. [PubMed: 19850107]

Rauch A, Rainer G, Logothetis NK. The effect of a serotonin-induced dissociation between spiking and perisynaptic activity on BOLD functional MRI. Proc. Natl. Acad. Sci. U. S. A. 2008; 105:6759–6764. [PubMed: 18456837]

Rostrup E, Law I, Blinkenberg M, Larsson HB, Born aP, Holm S, Paulson OB. Regional differences in the CBF and BOLD responses to hypercapnia: a combined PET and fMRI study. Neuroimage. 2000; 11:87–97. [PubMed: 10679182]

Shattuck DW, Mirza M, Adisetiyo V, Hojatkashani C, Salamon G, Narr KL, Poldrack RA, Bilder RM, Toga AW. Construction of a 3D probabilistic atlas of human cortical structures. Neuroimage. 2008; 39:1064–1080. [PubMed: 18037310]

Shirer WR, Ryali S, Rykhlevskaia E, Menon V, Greicius MD. Decoding Subject-Driven Cognitive States with Whole-Brain Connectivity Patterns. Cereb. Cortex. 2012; 22:158–166. [PubMed: 21616982]

Smith AJ, Blumenfeld H, Behar KL, Rothman DL, Shulman RG, Hyder F. Cerebral energetics and spiking frequency: The neurophysiological basis of fMRI. Proc. Natl. Acad. Sci. 2002; 99:10765–10770. [PubMed: 12134056]

Smith SM, Fox PT, Miller KL, Glahn DC, Fox PM, Mackay CE, Filippini N, Watkins KE, Toro R, Laird AR, et al. Correspondence of the brain's functional architecture during activation and rest. Proc. Natl. Acad. Sci. 2009; 106:13040–13045. [PubMed: 19620724]

Smith SM, Jenkinson M, Woolrich MW, Beckmann CF, Behrens TEJ, Johansen-Berg H, Bannister PR, De Luca M, Drobnjak I, Flitney DE, et al. Advances in functional and structural MR image analysis and implementation as FSL. Neuroimage. 2004; 23:208–219.

Spees WM, Lin T-H, Song S-K. White-Matter Diffusion fMRI of Mouse Optic Nerve. Neuroimage. 2013; 65:209–215. [PubMed: 23085108]

Sporns O, Tononi G, Kötter R. The human connectome: A structural description of the human brain. PLoS Comput. Biol. 2005; 1:0245–0251.

Tavor I, Parker Jones O, Mars RB, Smith SM, Behrens TE, Jbabdi S. Task-free MRI predicts individual differences in brain activity during task performance. Science. 2016; 352:216–220. [PubMed: 27124457]

Tettamanti M, Paulesu E, Scifo P, Maravita a, Fazio F, Perani D, Marzi Ca. Interhemispheric transmission of visuomotor information in humans: fMRI evidence. J. Neurophysiol. 2002; 88:1051–1058. [PubMed: 12163553]

Thomas BP, Liu P, Park DC, van Osch MJP, Lu H. Cerebrovascular reactivity in the brain white matter: magnitude, temporal characteristics, and age effects. J Cereb Blood Flow Metab. 2014

Viswanathan A, Freeman RD. Neurometabolic coupling in cerebral cortex reflects synaptic more than spiking activity. Nat. Neurosci. 2007; 10:1308–1312. [PubMed: 17828254]

Wang Y, Li T-Q. Analysis of Whole-Brain Resting-State fMRI Data Using Hierarchical Clustering Approach. PLoS One. 2013; 8:e76315. [PubMed: 24204612]

Waxman SG, Ritchie JM. Molecular dissection of the myelinated axon. Ann. Neurol. 1993; 33:121–136. [PubMed: 7679565]

Weber B, Fouad K, Burger C, Buck a. White Matter Glucose Metabolism during Intracortical Electrostimulation: A Quantitative [18 F] Fluorodeoxyglucose Autoradiography Study in the Rat. Neuroimage. 2002; 998:993–998.

Wilf M, Strappini F, Golan T, Hahamy A, Harel M, Malach R. Spontaneously Emerging Patterns in Human Visual Cortex Reflect Responses to Naturalistic Sensory Stimuli. Cereb. Cortex. 2015

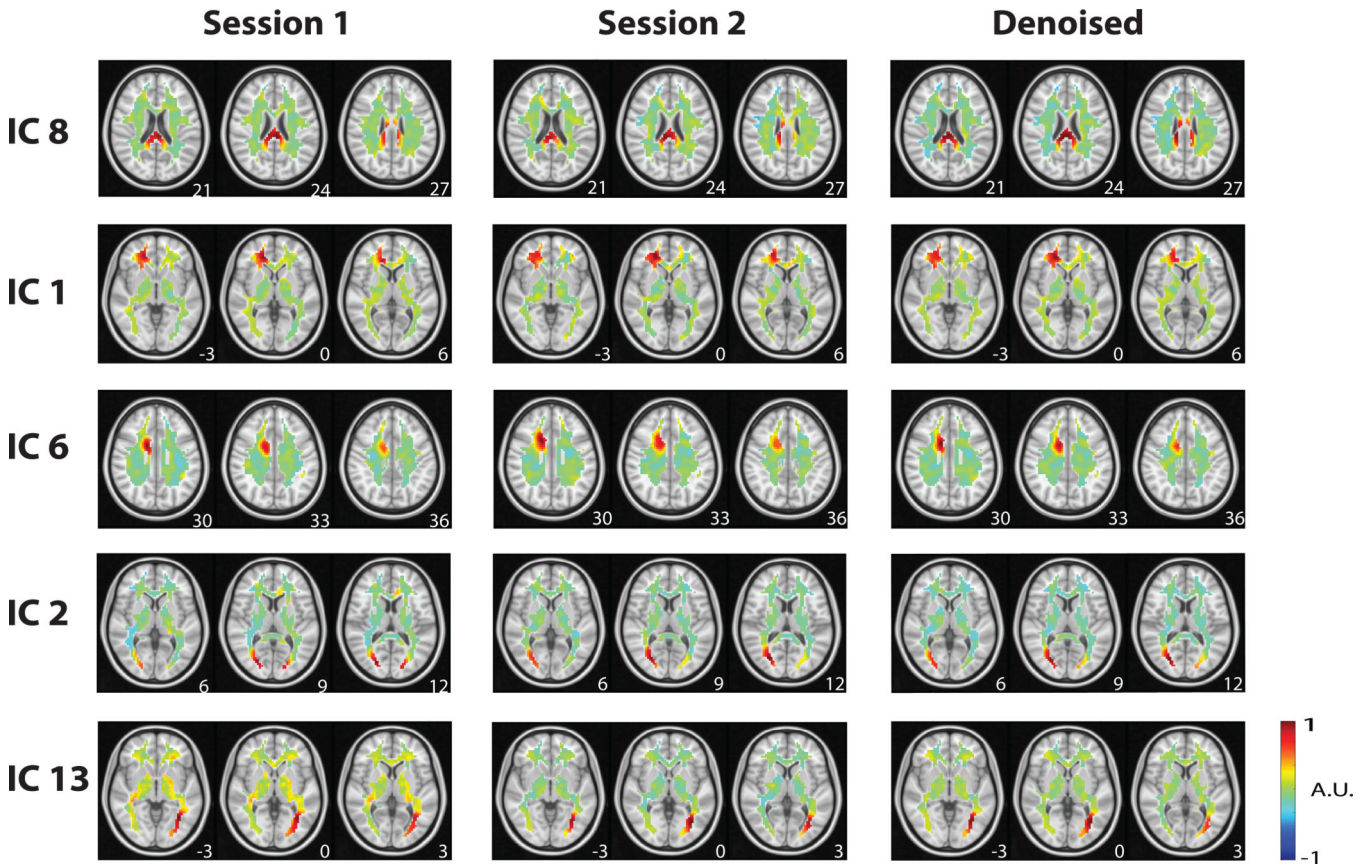

Figure 1. Reproducibility

A sample of reproducible components from Session 1 to Session 2, along with the corresponding de-noised components that consisted of information from both sessions. The z-coordinate (mm) of the position of each axial image is shown in the lower right corner. IC #8 corresponds to the posterior (splenium) corpus callosum. IC #1 corresponds to the right forceps minor. IC #6 corresponds to part of the cingulum. IC #2 corresponds to part of the optic radiations. IC #13 also corresponds to a part of the optic radiations.

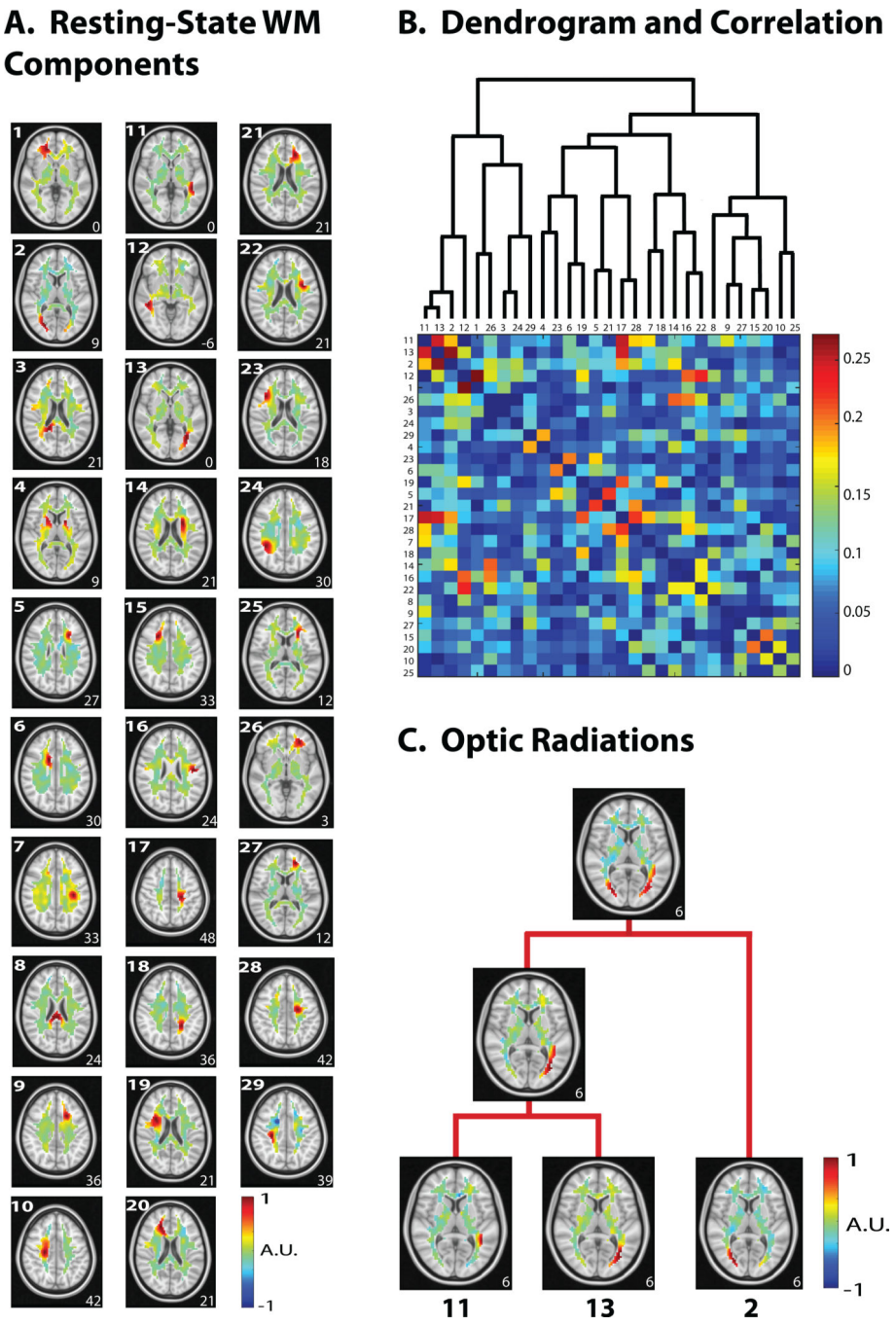

Figure 2. Hierarchical clustering of WM ICs in the resting state

A. 29 resting-state components were obtained after de-noising. **B**. The dendrogram used in the hierarchical clustering (top) with the corresponding temporal correlation values between WM ICs. **C**. Two portions of the left optic radiation were first clustered together, followed by clustering with a portion of the right optic radiation. For all axial slices in A and C, the z-coordinate (mm) is shown in the lower right corner.

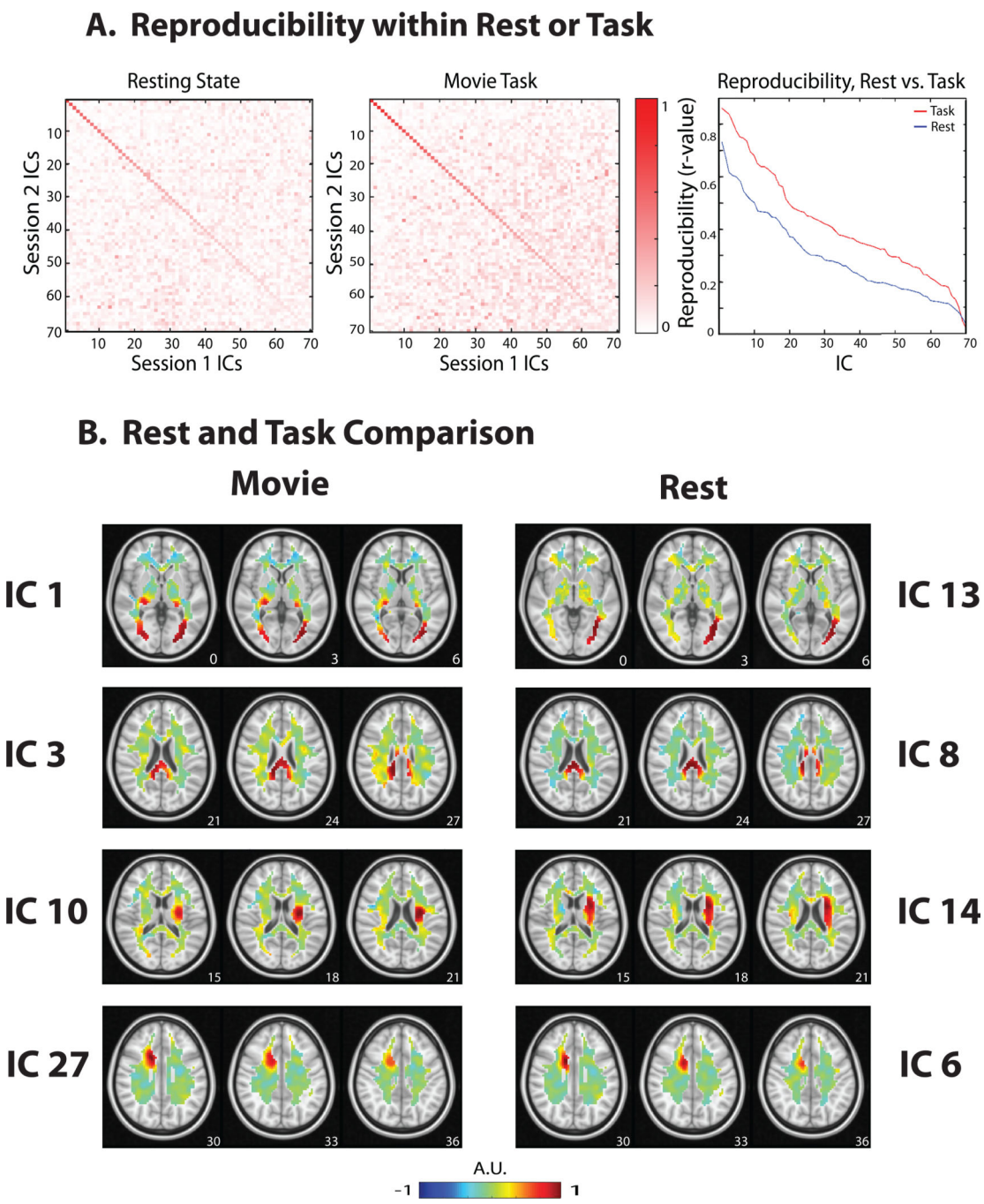

Figure 3. Reproducibility of ICA components

A. Reproducibility within the resting state or the task state. The spatial maps between session 1 and session 2 were optimally matched into pairs sorted in descending order of their spatial cross correlations. The matrices show the spatial correlations of one session's 70 components to the other session's 70 components, for either the resting state (left) or the movie task state (middle). The diagonal elements are the spatial correlations between individually 'paired' components. The 'paired' components generated by the movie task demonstrated stronger spatial correlations with one another than in the resting state (right).

B. Rest and task comparison of WM components. Four example pairs of components obtained from resting-state (right) and task-state (left) are shown. While the first row shows notably different maps, the other three rows show similar patterns. The z-coordinate (mm) of the position of each axial image is shown in the lower right corner.

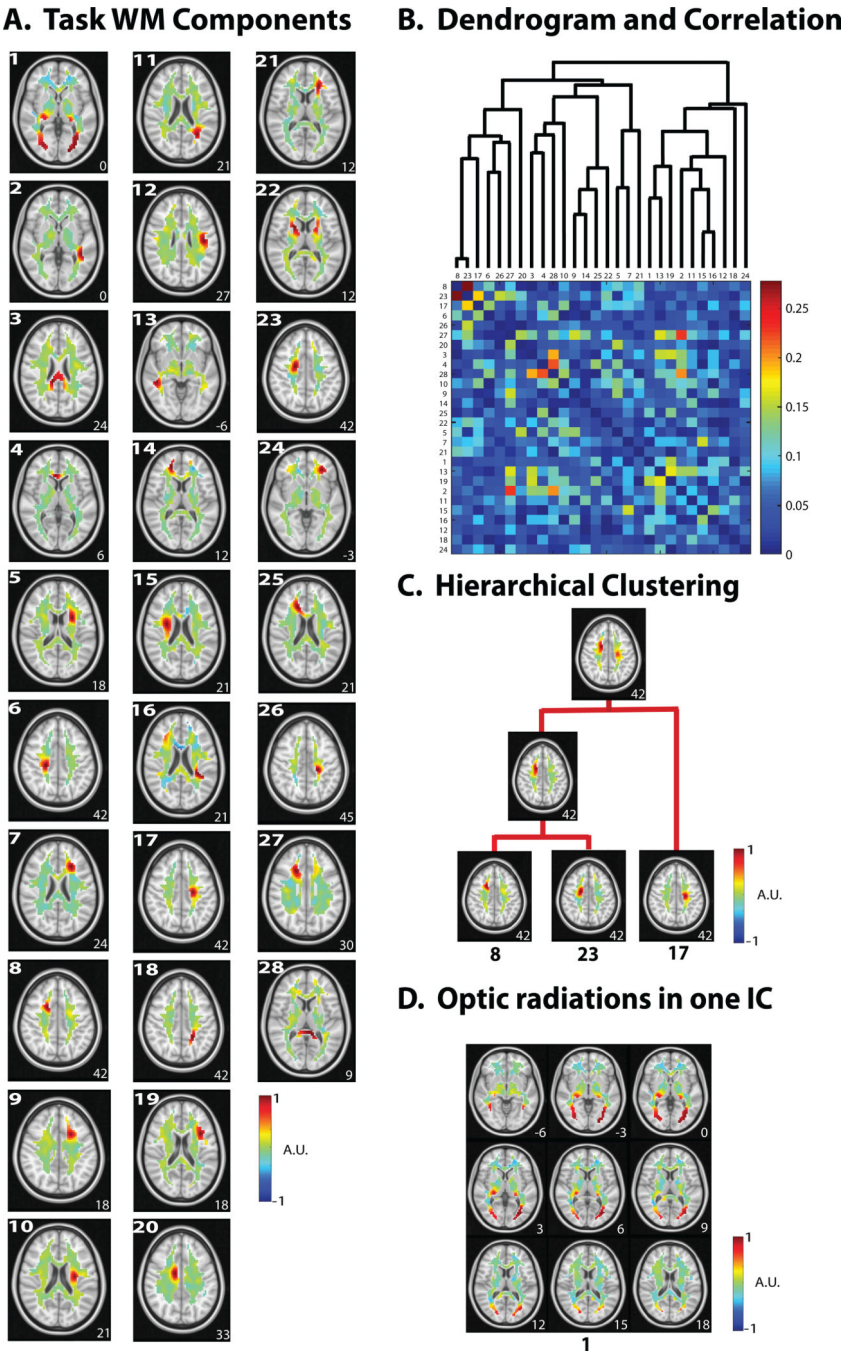

Figure 4. Task-state WM activity patterns

A. 28 task components were obtained after de-noising. The component number is shown in the top left corner. **B**. The dendrogram used in the hierarchical clustering (top) with the corresponding temporal correlation values between WM ICs during the naturalistic visual task. **C**. Hierarchical clustering of task unrelated components – (right anterior corona radiata). Two portions of a single tract were paired together, which were then paired with a more dorsal portion. **D**. Task-related component. One component shows the optic radiations

emanating from the LGN. For all axial slices in A, C, and D, the z-coordinate (mm) is shown in the lower right corner.

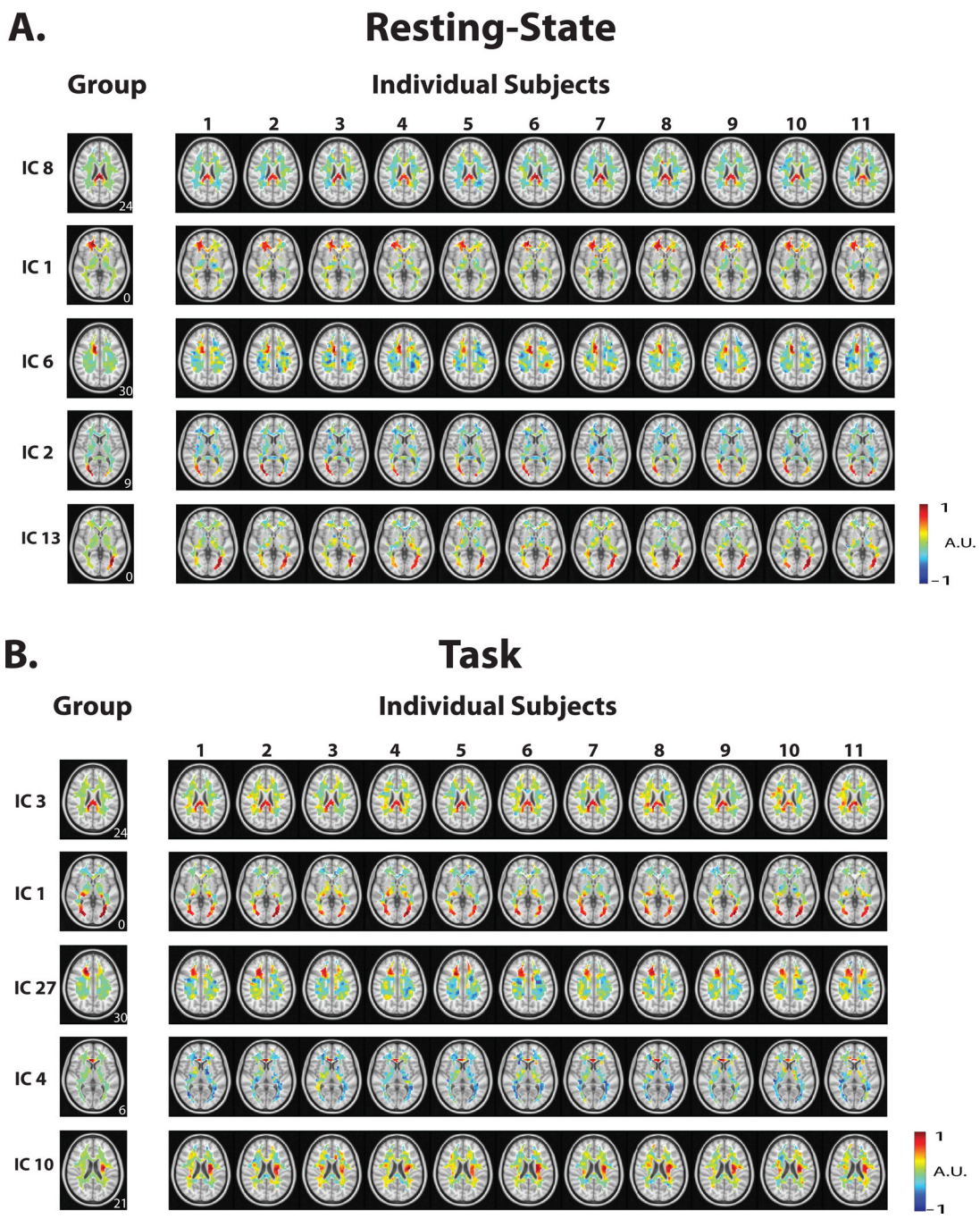

Figure 5.

ICA maps from individual subjects obtained through dual regression in resting-state (**A**) and during the task (**B**). For each state, the left-most column shows the group level map; the right columns show the map obtained from an individual subject using this method. The z-coordinate (mm) is shown in the lower right corner.

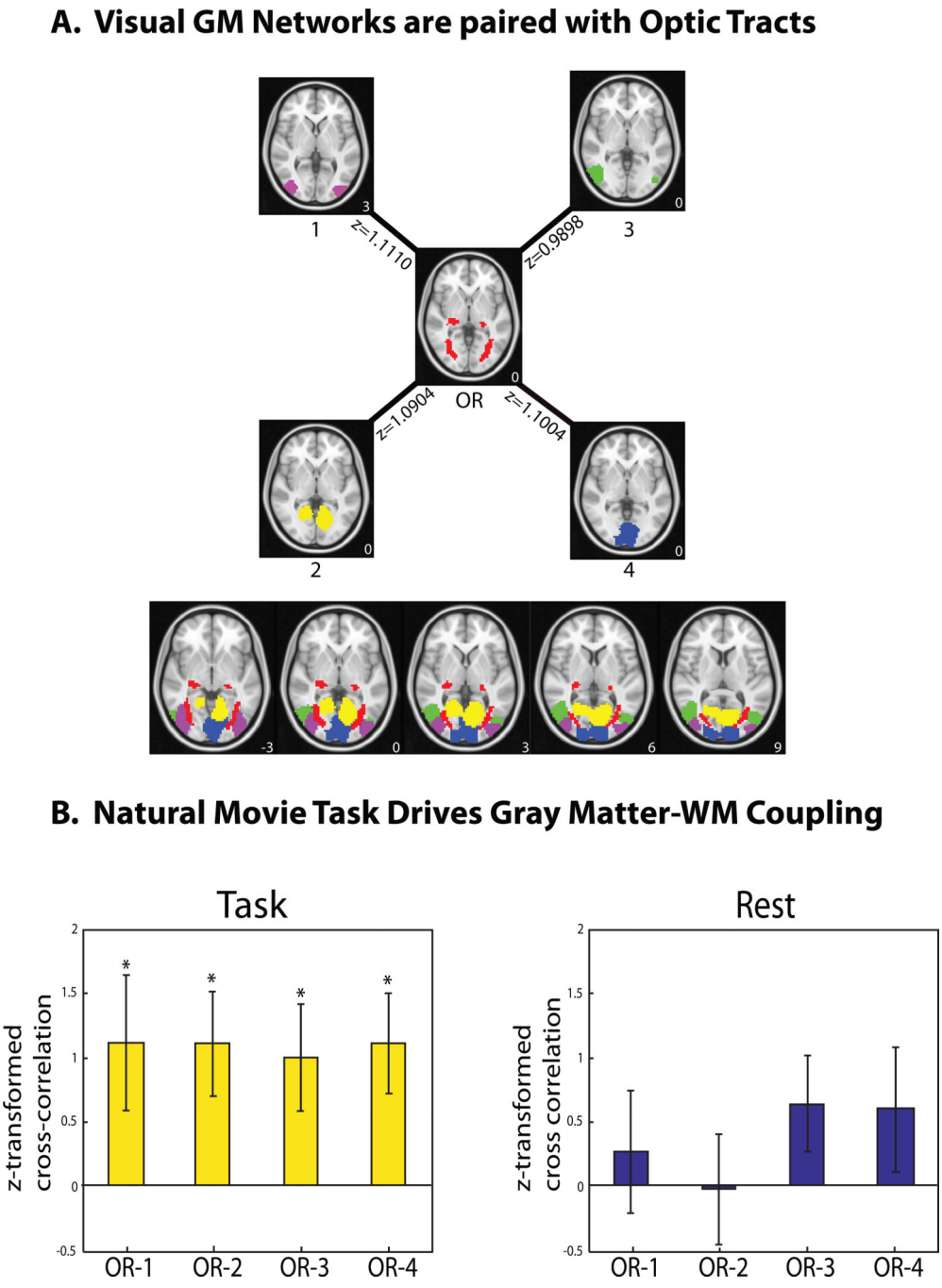

Figure 6.

Functional relationships between WM and GM networks. **A**. During natural visual perception, the optic radiations in WM (OR) were temporally correlated with four cortical visual networks in GM (ICs #1, #2, #3, and #4). Shown next to each connection is the average z-transformed cross correlation between the corresponding WM and GM regions. The z-coordinate (mm) is shown in the lower right corner. **B**. Such temporal correlations were statistically significant in the task state (left), but not in the resting state (right). These functional connectivity relationships are presented as OR-1 (i.e. optic radiations cross-

correlation with cortical visual IC #1), OR-2, OR-3, and OR-4. The bar height indicates the average z-transformed cross correlation. The error bar indicates the standard error of the mean.

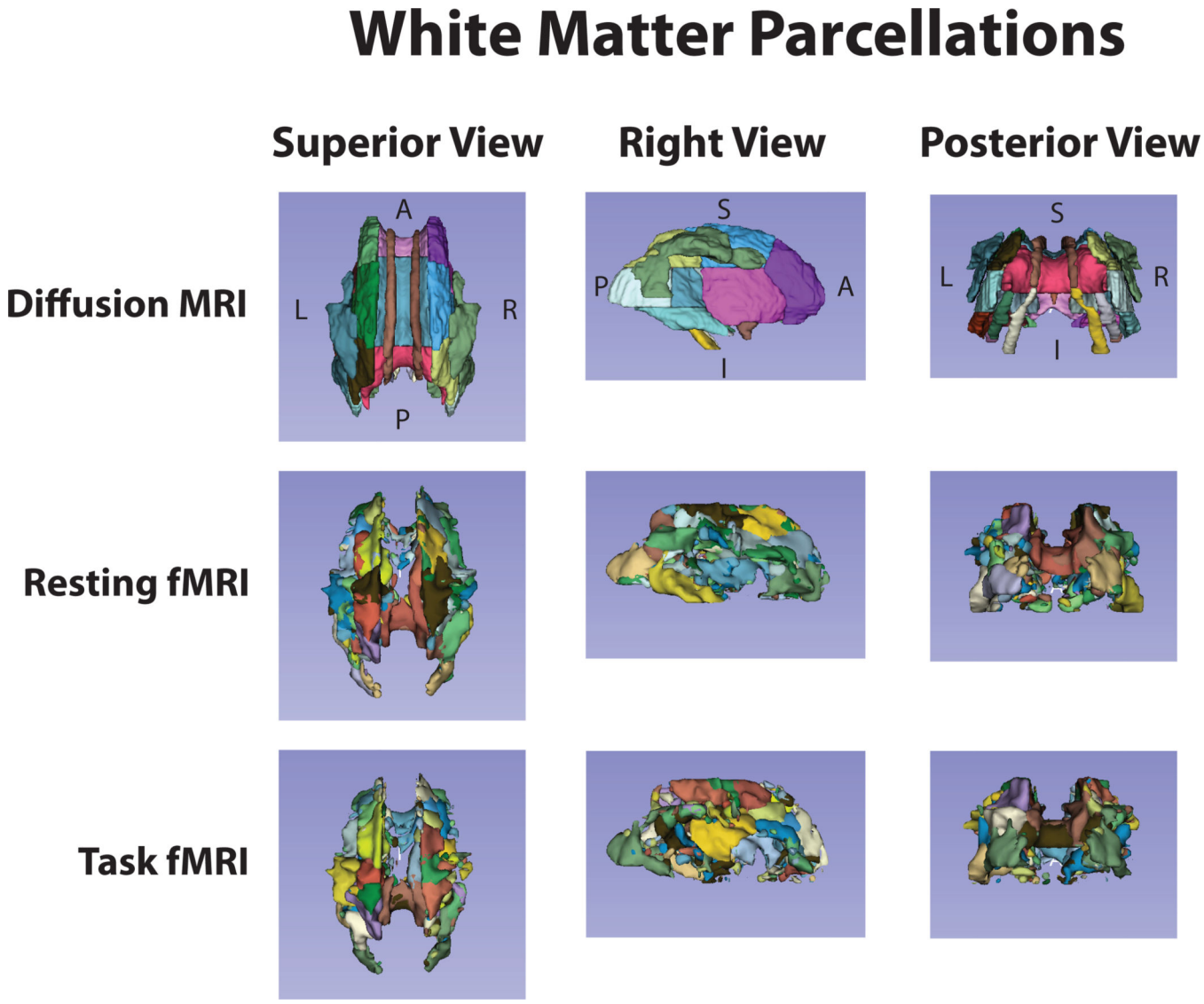

Figure 7. Structural vs. functional parcellation of the white matter

The first row shows the white-matter parcellation based on diffusion MRI (JHU ICBM-DTI-81 atlas). The second and third rows show the white-matter structures delineated from the thresholded ICA maps obtained from resting state fMRI or natural-vision task fMRI data, respectively.